

www.acsami.org Research Article

Thiotetrelates Li₂ZnXS₄ (X = Si, Ge, and Sn) As Potential Li-Ion Solid-State Electrolytes

Jiajie Zhong, Bingkai Zhang,* Feng Pan,* and Zhan Lin*



Cite This: ACS Appl. Mater. Interfaces 2022, 14, 9203-9211



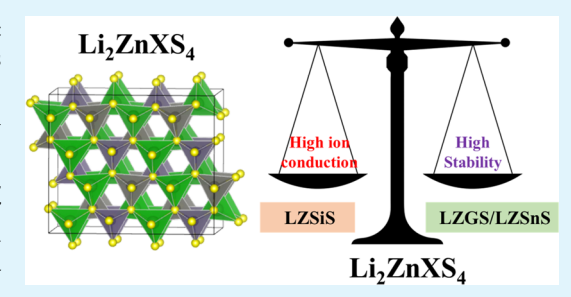
ACCESS

Metrics & More

Article Recommendations

s Supporting Information

ABSTRACT: A novel inorganic solid-state electrolyte (ISSE) with high ionic conductivity is a crucial part of all-solid-state lithium-ion (Li-ion) batteries (ASSLBs). Herein, we first report on Li_2ZnXS_4 (LZXS, X = Si, Ge, and Sn) semiconductor-based ISSEs, crystallizing in the corner-sharing tetrahedron orthorhombic space group, to provide valuable insights into the structure, defect chemistry, phase stability, electrochemical stability, $\text{H}_2\text{O}/\text{CO}_2$ chemical stability, and Li-ion conduction mechanisms. A key feature for the Li-ion transport and low migration barrier is the interconnected and corner-shared [LiS $_4$] units along the *a*-axis, which allows Li-ion transport via empty or occupied tetrahedron sites. A major finding is the first indication



that Li-ion migration in $\text{Li}_2\text{ZnSiS}_4$ (LZSiS) has lower energy barriers (\sim 0.24 eV) compared to $\text{Li}_2\text{ZnGeS}_4$ (LZGS) and $\text{Li}_2\text{ZnSnS}_4$ (LZSnS), whether through vacancy migration or interstitial migration. However, LZGS and LZSnS exhibit greater $\text{H}_2\text{O}/\text{CO}_2$ stability compared to LZSiS. The novel framework of LZXS with relatively low Li-ion migration barriers and moderate electrochemical stability could benefit the ASSLB communities.

KEYWORDS: Li₂ZnXS₄, defect chemistry, stability, lithium-ion conductivity, sulfide solid-state electrolyte, all-solid-state lithium-ion battery

1. INTRODUCTION

Lithium-ion (Li-ion) batteries are being investigated to help convert a conventional vehicle into an electric vehicle. High capacity and high safety to ensure the safety of Li-ion batteries are the utmost requirements for an electric car. 1-5 The allsolid-state Li-ion batteries (ASSLBs) require solid-state electrolytes (SSEs) that exhibit good Li-ion conductivity and electrochemical stability. 6-10 In the last decade, major efforts have been reported toward the exploration of new fast Li-ion conductors, leading to several typical inorganic SSEs (ISSEs), such as $\text{Li}_{10}\text{GeP}_2\text{S}_{12}$ (LGPS), 11,12 $\text{Li}_6\text{PS}_5\text{Cl}$ (LPSCl), 13,14 $\text{Li}_{1.3}\text{Al}_{0.3}\text{Ti}_{1.7}(\text{PO}_4)_3$, $^{15-17}$ and $\text{Li}_7\text{La}_3\text{Zr}_2\text{O}_{12}$ (LLZO). 18,19 Although compared to organic liquids or polymer electrolytes, the Li-ion transport of ISSEs in ASSLB setups is not satisfactory because of the following reasons: the ionic conductivity of ISSEs is less than that of organic liquids or polymer electrolytes at room temperature, poor interfacial incompatibility between cathodes/anodes and ISSEs, and the poor electrochemical stability of ISSEs.^{20–23} Hence, it is necessary to find new ISSE materials with the following characteristics: low electron conduction, high ion conduction, and good electrochemical/chemical stability.²⁴

Recently, a class of quaternary diamond-like semiconductors, Li_2ZnXS_4 (LZXS, X = Si, Ge, and Sn), crystallizing in the polar, noncentrosymmetric orthorhombic space group $Pna2_1$, are used as nonlinear optical materials in the optical frequency conversion field. The connectivity of point-shared LiS₄ tetrahedrons, the wide band gap, and the polarizability of host

atoms in LZXS may well make them ideal for use in SSE materials. However, to date, they have not been studied in the context of Li-ion migration and electrochemical stability. Many basic issues, such as the Li-ion diffusion structure, defect chemistry, chemical/electrochemical stability, $\rm H_2O/CO_2$ stability, the Li-ion migration mechanism, and the Li-ion migration barrier, need to be checked if LZXS are acceptable as ISSEs.

In this work, we first use the first-principle calculations combined with density functional theory (DFT) to compute the bulk formation energies of crystal structures as available in the material project as "computer experiments" to evaluate the crystal structure, stability (against phase decomposition, H_2O/CO_2 corrosivity, voltage, and cathode materials), and, most importantly, Li-ion conductivity in this system. The technique has shown great success and has many advantages, such as rapid evaluation and prediction of fast ionic conductors before their experimental realization and high accuracy of physical properties.

Received: December 14, 2021 Accepted: January 21, 2022 Published: February 8, 2022





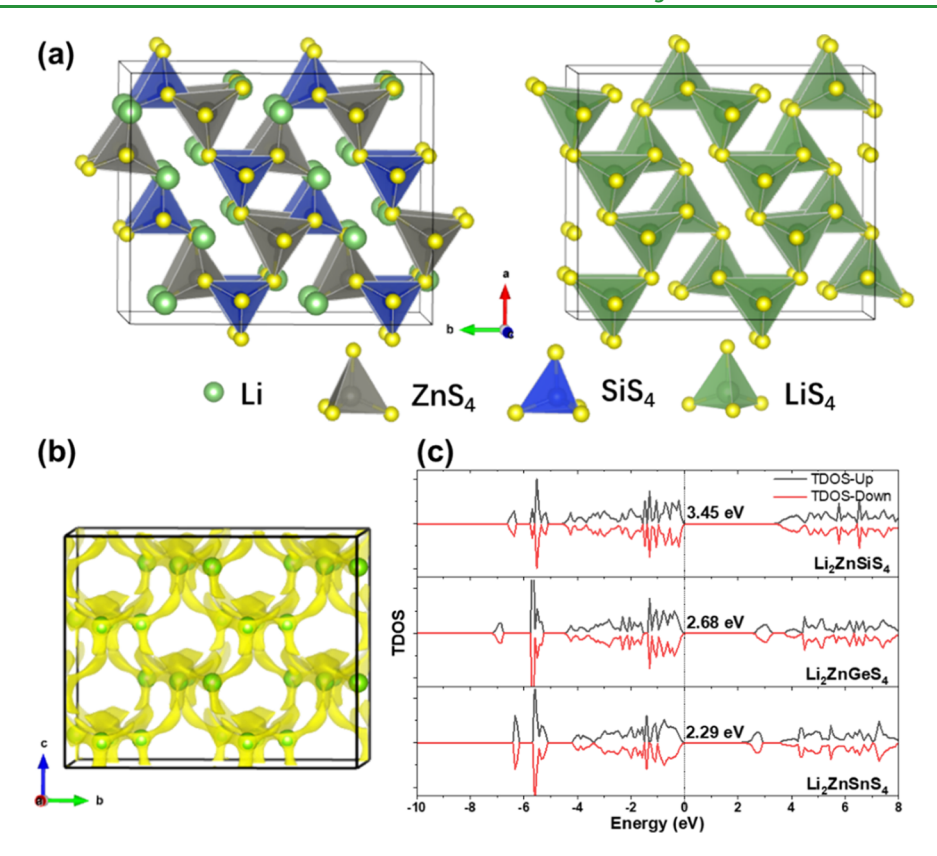


Figure 1. (a) Side view of the LZXS crystal structure in different structural unit views. (b) Li diffusion channel is determined by the yellow BV isosurfaces, which are regarded as the continuous network for Li-ion diffusion. (c) Calculated TDOS of LZXS. The Fermi level (dashed line) is set to be zero. The green spheres, gray, green, and blue tetrahedrons represent the Li atoms, [LiS₄], [ZnS₄], and [SiS₄] units, respectively.

2. COMPUTATIONAL DETAILS

DFT with a general gradient approximation applying the Perdew–Burke–Ernzerhof (PBE) functional, 28,29 as implemented in the program of Vienna Ab initio Simulation Package, is used for all the total energy calculations. The electronic wave functions of valence electrons are expanded via the projector-augmented wave basis set. The Monkhorst–Pack k-point sampling method is carried out for all calculations (for the (1 \times 2 \times 2) LZXS supercell, 3 \times 2 \times 2 k-point samplings are used). The cutoff energy of 500 eV, residual force less than 0.01 eV/Å, and total energy less than 2.0 \times 10 $^{-5}$ eV are utilized for all the calculations. The vacancy and interstitial migration are carried out using the climbing image nudged elastic band (Cl-NEB) method. The climbing image nudged core—hole method. The details of the defect formation energy refer to the Computation Section of the Supporting Information.

The phase diagram, electrochemical stability window, interfacial stability of LZXS with various cathodes, and $\rm H_2O/CO_2$ stability of LZXS are determined using grand canonical linear programming (GCLP) and the open quantum materials database (OQMD). ^{33,34} More information about GCLP and the OQMD is detailed in previous studies. ^{35–39} The GCLP makes out the decomposition or reaction equations from the reactants into all the possible products and seeks the minimum energy solution under the constraint that the stoichiometric coefficient of chemical reaction must be positive. The decomposition energy of LZXS, $E_{\rm decomp}$, is defined as

$$E_{\text{decomp}} = [E(\text{products}) - E(\text{LZXS})]/n_{\text{atoms}}$$
(1)

For the interfacial stability of LZXS in contact with the cathode, the $\Delta E_{\text{mixing-energy}}$ of the reaction of (1-x)cathode + xLZXS $\rightarrow C_{\text{equilibrium}}$ is calculated and defined as

$$\Delta E_{\text{mixing-energy}} = [E(C_{\text{equilibrium}}) - (1 - x)E(LZXS) - xE(\text{cathode})]/n_{\text{atoms}}$$
(2)

where $C_{\rm equilibrium}$ is the thermodynamic stable phase equilibrium specified from a compositional phase diagram, x is the mixing parameter, which can vary between 0 and 1, and $n_{\rm atoms}$ represents the equal number of atoms for each reactant in the reaction. To study the H_2O/CO_2 chemical stability of LZXS, the $\Delta E_{\rm mixing-energy}$ of the following two reactions are calculated, xLZXS + $(1-x)H_2O/CO_2 \rightarrow C_{\rm equilibrium}$, and are defined as

$$\Delta E_{\text{mixing-energy}} = [E(C_{\text{equilibrium}}) - (1 - x)E(H_2O/CO_2) - xE(LZXS)]/n_{\text{atoms}}$$
(3)

where the meanings of $C_{\rm equilibrium}$, x, and $n_{\rm atoms}$ have been stated in eq 1. A negative value of $\Delta E_{\rm mixing-energy}$ or $E_{\rm decomp}$ indicates that the mixing or decomposition reactions are thermodynamically favorable ones.

3. RESULTS AND DISCUSSION

3.1. Structure Modeling, Defect Chemistry, and Phase Stability. The starting point of the work is to reproduce the experimentally observed Li₂ZnGeS₄ (LZGS) crystal structure. Then, the optimized LZGS compound is used as the parent structure for modeling Li₂ZnSiS₄ (LZSiS) and Li₂ZnSnS₄ (LZSnS) ones (Figure 1a). The LZXS crystallizes in the *Pna*2₁ space group of orthorhombic systems with lattice

constants. The volume of the $[LiS_4]$, $[ZnS_4]$, and $[XS_4]$ units in three LZXS compounds is listed in Table 1. The calculated

Table 1. Calculated Structural Parameters in the LZXS System²⁵⁻²⁷

X	a (Å)	b (Å)	c (Å)	(\mathring{A}^3)	$ZnS_4 (\mathring{A}^3)$	$Li(1)S_4$ and $Li(2)S_4$ (Å ³)
Si	6.50	7.85	6.22	5.07	6.77	7.22, 7.79
Ge	6.60	7.94	6.30	5.86	6.76	7.25, 7.81
Sn	6.79	8.05	6.44	7.34	6.81	7.45, 7.75

lattice parameters underestimate experimental lattice parameters by 2-4% on average. 25-27 The detailed structural parameters with atom positions are shown in Table S1 of the Supporting Information. In the asymmetric unit, there are two unique Li sites because of the distribution of their in-layer tetrahedral neighbors: ZnS4 and XS4, one Zn atom, one Si atom, and four S atoms. All the Li, Zn, and Si atoms have four coordination with S atoms to form tetrahedrons, and all of the tetrahedrons connect with each other by the way of corner sharing. LZXS shows two sequences along the a-axis: (i) $Li(1)S_4-Li(2)S_4-Li(1)S_4-Li(2)S_4$ and (ii) ZnS_4-XS_4- ZnS4-XS4. The orientation of both sequences is almost parallel, and the two sequences are arranged in an alternating way along the *b*-axis. To further determine the Li-ion diffusion pathway, the crystal-chemical bond-valence (BV) theory of ionic and covalent bonding is introduced, in which the accessible sites for Li-ions are determined by the valence mismatch of Li-ions (Figure 1b).⁴⁰ Figure 1b shows possible three-dimensional (3D) Li-ion migration pathways in this structure. Therefore, LZXS compounds possess diamond-like structures and visible 3D diffusion channels for lithium diffusion. The comparison of calculated structural parameters in Table 1 shows lattice constants, XS4, and LiS4 volumes increase with larger X-site atoms (Si < Ge < Sn) in LZXS, which may be correlated with Li-ion conductivity and the Liion migration barrier. 11,41 The total electronic densities of states (TDOS) presented in Figure 1c shows that LZXS compounds have a wide band gap with the values of 3.45 eV (LZSiS), 2.68 eV (LZGS), and 2.29 eV (LZSnS). Therefore, LZXS has an insulating nature, indicating that the dense LZXS compounds are unfavorable for electronic conduction. We should, however, note that the ionic and electronic conduction of LZXS is also dependent on the type and amount of the defects (the TDOS of defected LZSiS are shown in Figure S1 in Supporting Information).

To identify the dominant defects or diffusion carriers in LZXS, calculations on intrinsic defects in LZXS compounds are done on the optimized structures. The three types of defects, namely a Li vacancy ($V_{\rm Li}$), a Li interstitial (Li_i), and a Li Frenkel pair (vacancy-interstitial) (Li_{FP}), are introduced; the corresponding neutral defect formation energies at 0 V (see eq S1 in the Supporting Information) are given in Table 2. From the formation energies in the table, Li interstitial formation

Table 2. Calculated Formation Energies of a Neutral Defect in the $(1 \times 2 \times 2)$ LZXS Supercell at 0 V

LZXS	Li vacancy (eV)	Li interstitial (eV)	Li Frenkel (eV)
Si	3.72	1.18	1.38
Ge	3.78	0.28	1.77
Sn	3.83	0.04	1.80

processes are more favorable than the formation of the vacancy and Frenkel defect. The large positive value of Li vacancy, that is, 3.72-3.83 eV, suggests that the Li vacancy in LZXS is hard to achieve and there are limited concentrations of Li vacancy in this system. The formation energies of the three defects are also calculated considering neutral, negative, and positive charge states as shown in Figure 2a—c, within the voltage range of typical Li-ion batteries of 0-4.5 V. It is seen from Figure 2 that on the anode side, the neutral (Li,) and positive Li interstitial (Li_i⁺) defects have the lower formation energies. On the cathode side, the neutral Li vacancy (V_{Li}) , positive Frenkel pair (FP_{Li}⁺), and positive Li interstitial (Li_i⁺) have lower formation energies (eV). Figure 2d indicates the domain defects of LZXS with the change of applied voltage. It is important to note that the concentrations of defects in LZXS can be introduced into this system by obtaining offstoichiometric compositions $Li_{2+2x}Zn_{1-x}XS_4$ with x > 0 or doping $(AI/Ga)^{3+}$, $(P/As)^{5+}$ at X^{4+} sites to obtain Li interstitial or Li vacancy defects, respectively.

3.2. Electrochemical/Interfacial Stability and H₂O/ CO₂ Chemical Stability. We first evaluate the phase stability and electrochemical stability with respect to all the possible decomposed crystalline materials at 0 K computed from the DFT-based database combined with the GCLP method. 42-45 In the phase diagram of Li₂S-XS₂-ZnS compounds (see Figure 3a-c), there is only one decomposition combination for both LZSiS and LZGS compounds (Li₂ZnSiS₄ → ZnS + Li_2SiS_3 and $2\text{Li}_2\text{ZnGeS}_4 \rightarrow 2\text{ZnS} + \text{GeS}_2 + \text{Li}_4\text{GeS}_4$), and two decomposition combinations for the LZSnS compound $(\text{Li}_2\text{ZnSnS}_4 \rightarrow \text{ZnS} + \text{SnS}_2 + \text{Li}_2\text{S} \text{ and } 2\text{Li}_2\text{ZnSnS}_4 \rightarrow 2\text{ZnS}$ + SnS_2 + Li_4SnS_4). In the two combinations for LZSnS, the latter one is the more favorable case. Also, the decomposition energies (see eq 1 in the Computational Details) for LZGS and LZSnS with respect to decomposition products are negative with values of -0.06 and -0.05 eV/atom, respectively, suggesting they are in their low energy state against decomposition into smaller compounds. However, the decomposition of LZSiS with respect to decomposition products has a positive decomposition energy of 0.08 eV/ atom. Phase stability for phases on the hull is quantified by the difference in the formation energy between the compound and its lowest energy state using the phase stability analysis tools contained in Pymatgen. The formation energy above the convex hull (E_{hull}) is a measure of the driving force for the compound decomposition. The calculated E_{hull} values for LZSiS, LZGS, and LZSnS are 0.27, 0.29, and 0.30 eV/atom, respectively. The predicted instability greater than 0.20 eV/ atom above the convex hull needs to be evaluated using an experimental setup over a long operating time. In addition, for the decomposition reaction of $Li_{10}GeP_2O_{12}$ (LGPO) \rightarrow Li₃PO₄ + Li₄GeO₄, the decomposition energy is 0.10 eV/ atom, which is larger than that of LZSiS (0.08 eV/atom). However, this point does not hinder its assemblage in a battery setup, where the kinetic barriers of decomposition reaction might matter. 46 Therefore, the solid-solid decomposition reaction for metastable LZXS compounds would be less problematic in practice.

The electrochemical stability of ISSE materials is very important while in contact with negative or positive electrodes. Figure 3d-f shows the electrochemical stability window of LZXS and the phase equilibria within the voltage range of 0-5 V. We note that LZSiS would decompose into Li₂SiS₃ and ZnS in the range of 1.42-2.30 V (the yellow-shaded region);

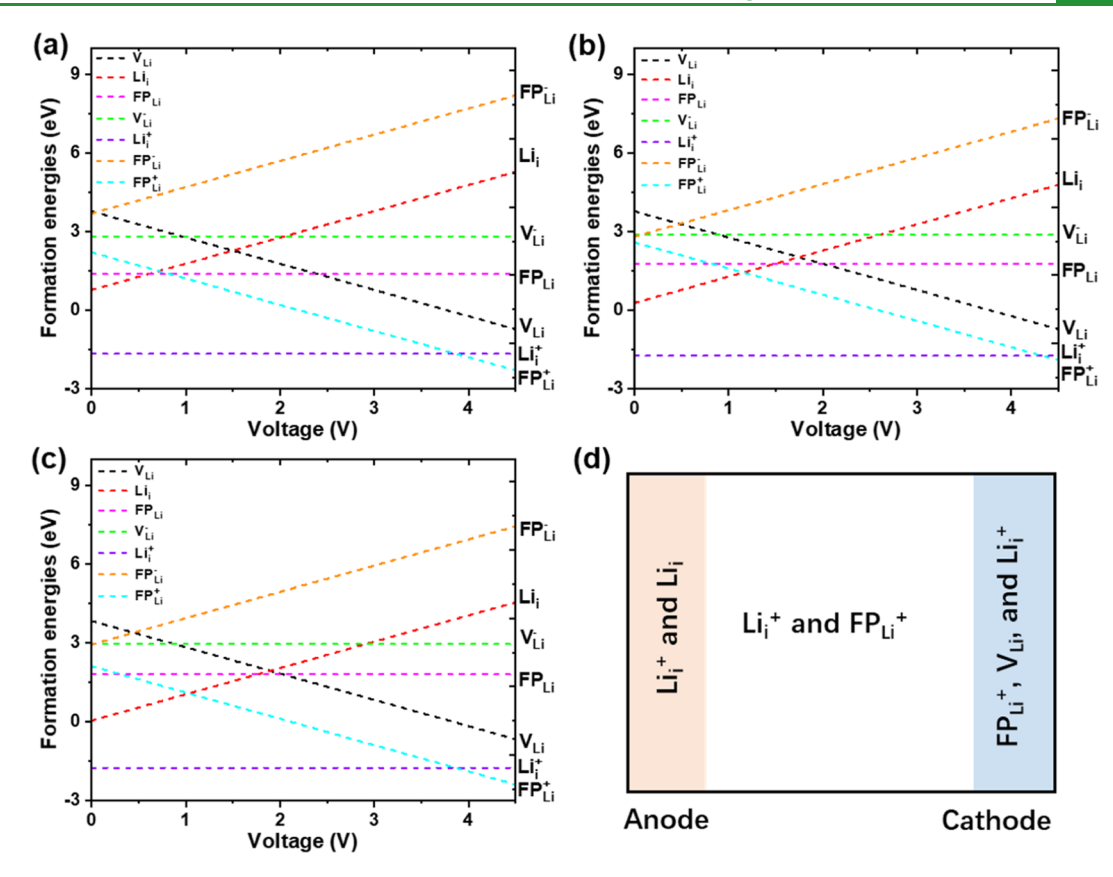


Figure 2. (a-c) Formation energies, $E_f(i,q)$ for all the six point defects in LZSiS, LZGS, and LZSnS, respectively. (d) Schematic figure shows the dominant defects within LZXS with the change of voltage.

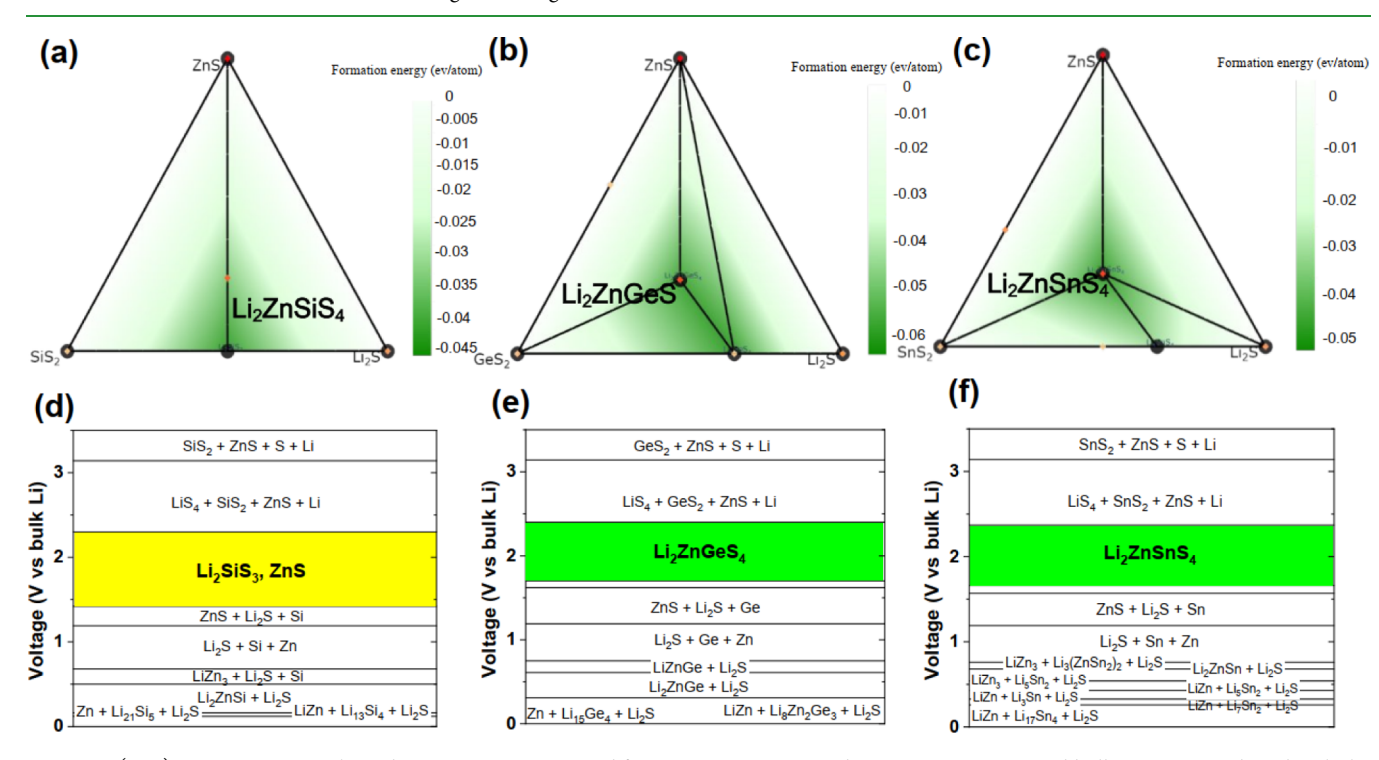


Figure 3. (a-c) Li₂S-XS₂-ZnS phase diagram at 0 K computed from LZnSiS, LZGS, and LZSnS DFT-computed bulk energies combined with the crystal database, respectively. The different shades of green represent different formation energy values. The deeper the color, the more negative the formation energy. (d-f) Voltage profile and phase equilibria of LZnSiS, LZGS, and LZSnS upon lithiation and delithiation are determined using GCLP and the OQMD. The yellow- or green-shaded regions suggest the electrochemical stability window of LZXS.

although LZGS and LZSnS compounds can maintain phase stability in the range of 1.70-2.40 and 1.66-2.38 V (the

green-shaded regions), respectively. Although LZSiS would decompose into Li₂SiS₃ and ZnS, it does not mean it has poor

electrochemical stability. It has been proven that most of the ISSE materials rely on the formed solid-electrolyte interphase (SEI), which can prevent the further spread of electrochemical decomposition reactions. 47-49 The self-decomposition compound Li₂SiS₃ (with a band gap of ~3.2 eV) being an ionic conductor and electron insulator can facilitate Li-ion diffusion and block the electron transport.⁵⁰ Meanwhile, the formed SEI also includes metallic elements, which can conduct electrons and thus reduce the stability of the interface. Thus, the exact electrochemical windows need to be proven by experiments. Doping Al element into LZXS could tune Li contents and the host of LZXS, which are correlated to ion conductivity. Thus, in addition to the stoichiometric structure, we also calculate the Al-doped LZXS system and LGPS (Figure S2 in the Supporting Information). We found that LZXS compounds exhibit a wider electrochemical stability window compared to Al-doped LZXS and LGPS (Figure 4).

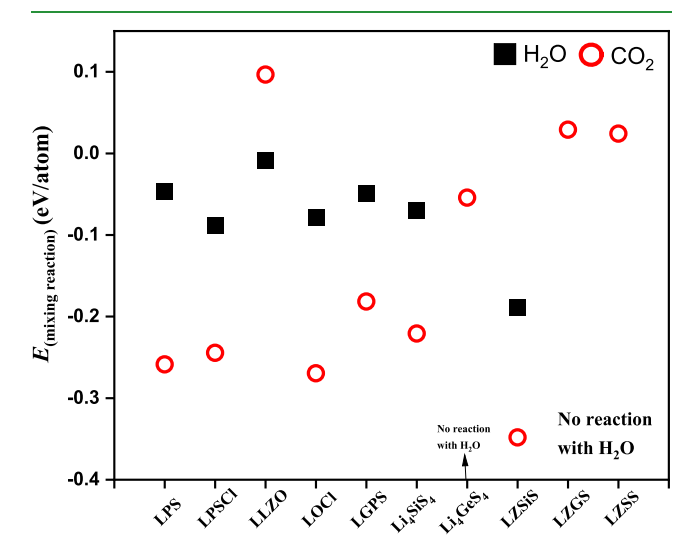


Figure 4. H_2O/CO_2 stability for LZXS and other ISSEs (for comparison) are shown. Li₃PS₄, LPSCl, and LOCl.

To understand the interfacial electrochemistry of LZXS compounds with various cathodes, namely, $LiMO_2$ (M = Co, Ni, and Mn), LiFePO₄, LiTiS₂, and LiVS₂, the electrochemical/chemical reaction: xcathode + (1 - x)LZXS \rightarrow $C_{\text{equilibrium}}$ (see eq 2 in the method), is considered in the following part. The thermodynamically feasible chemical reactions between LZXS and the cathode are detailed in Tables S2-S7 in the Supporting Information. We found that mixing chemical reactions at the oxide cathode/LZXS interface are thermodynamically favorable and form various reaction products, which could be detrimental to cyclability. However, there is no mixing reaction of LZXS with phosphate (LiFePO₄) and sulfide cathodes (LiTiS₂ and LiVS₂) at their cathodic voltage limit. The poor ionic conduction and good electron conduction of mixing reaction product compositions suggest LZSiS exhibits poor interfacial compatibility with oxide cathodes, which is like that found for LGPS. The air-sensitive or chemical reactivity of sulfide ISSEs, that is, the H₂O/CO₂induced chemical reaction with the products of H₂S/Li₂CO₃, is one main obstacle to commercial application. Therefore, to determine the H2O and CO2 stability of LZXS, we consider the following reactions: $xLZXS + (1 - x)H_2O/CO_2 \rightarrow$ $C_{\text{equilibrium}}$ (see eq 3 in the method), and tabulate the expected reaction products while considering typical oxide and sulfide

ISSEs, revealing the difference compared to oxide materials. According to the definition, a negative value suggests the thermodynamic equilibrium to C_{equilibrium} generation. Tables S8 and S9 in the Supporting Information show the chemical reaction equations with the maximum reaction energies between the ISSE compounds and H₂O/CO₂ molecular into possible products. We found that most ISSEs (all sulfides, Li₃OCl (LOCl), and LLZO) would react with H₂O/CO₂ with negative mixing reaction energies, except LiTi₂(PO₄) and Li₃PO₄. We note that the extent of H₂O/CO₂ chemical instability for LZSiS (-0.19 and -0.37 eV/atom) is close to that of LGPS (-0.09 and -0.25 eV/atom). However, there is no reaction between LZGS and LZSnS with H₂O. The moisture stability of the LZXS follows the rules of the hard and soft acids and bases theory; that is, hard acid Si prefers to replace the soft base S with hard base O, but soft acid Ge/Sn prefers to react with soft base S. We note that LZGS and LZSnS also exhibit better CO₂ stability compared to other sulfide ISSEs, Li₅AlO₄ and Li₅GaO₄. This good stability characteristic of LZGS and LZSnS against H₂O and CO₂ would favor a stable performance as soon as they are exposed to air and moisture. But, the thermodynamic H₂O and CO₂ instability of LZSiS should be regarded as preventing it from contacting with air during the process of making powder.

3.3. Li-lon Mobility in LZXS. DFT-based Cl-NEB calculations can determine the migration barrier along the migration path. Thus, to understand the Li-ion migration mechanisms in the LZXS system, the Cl-NEB calculations of the Li direct hopping via vacancy migration and interstitial migration in LZXS are performed along the pathway consisting of corner-shared [LiS₄] chains shown schematically in Figure 5a,c, respectively. First, Li direct hopping via Li vacancy migration along the a-axis direction in LZXS is calculated. Herein, we consider four Li positions as illustrated in Figure 5a, with Li-ions passing through the empty tetrahedral Li sites in the LiS₄ unit layer. These four Li sites are structurally very similar and have a very small difference in site energy (Si: 0.03 eV, Ge: 0.01 eV, and Sn: 0.01 eV) because of the two Li sites in LZXS. The migration barrier of Li vacancy in LZSiS, LZGS, and LZSnS is ~ 0.24 , ~ 0.32 , and ~ 0.41 eV (Figure 5b), respectively. The migration barrier of Li vacancy in LZSiS is comparable to the value of ~0.21 eV measured for the LGPS. 12,46,51 Second, the Li interstitial migration along the aaxis in LZXS is calculated (Figure 5c,d). The migration barrier of interstitial migration in LZSiS, LZGS, and LZSnS is ~0.20, ~0.31, and ~0.51 eV, respectively, indicating that the migration barrier of interstitial migration is comparable to that of Li direct hopping via vacancy. We note that the formation energy of Li interstitials is lower than that of Li vacancy. Thus, the interstitial migration mechanism is the energetically favored one in this structure. Compared to aliovalent substitutions, isovalent ones can have significant impacts on ion dynamics, which shows that formation energies and potential energy landscapes differ when going from Si to Sn. In addition, the finding that small host cations are correlated with reduced migration in LZXS is consistent with that in $\text{Li}_{10}\text{MP}_2\text{S}_{12}^{-11}$ but in contrast to that in $\text{LiM}_2(\text{PO}_4)_3^{-52}$ (X = Si, Ge, and Sn).

The difference in the interaction between Li and S sublattice and the hybridization between X and S may explain why LZSiS has a significantly lower migration barrier compared to LZGS and LZSnS. The hybridization between transition metals and oxygen has been reported to play a critical role in lithium

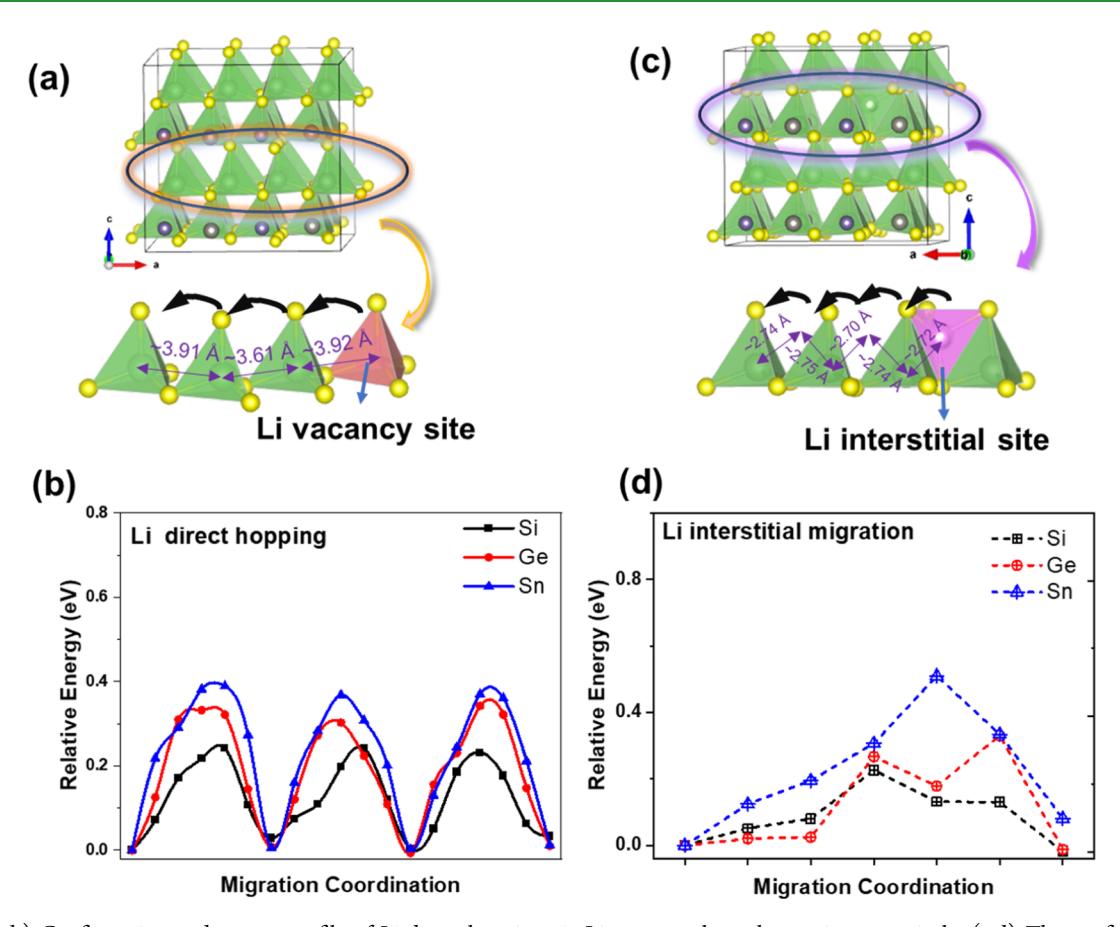


Figure 5. (a,b) Configuration and energy profile of Li direct hopping via Li vacancy along the a-axis, respectively. (c,d) The configuration and energy profile of Li interstitial migration via interstitial sites along the a-axis, respectively. The green tetrahedrons represent the [LiS₄] units.

intercalation voltages and the activity of oxygen electrocatalysts.⁵³ Valuable hybridization information can be gleaned from crystal orbital Hamilton population (COHP), which often provide insight into bonding—antibonding interaction energy regions of the material. Figure 6a—c exhibits COHP for the X-S interactions in the bulk LZXS. Figure 6d shows the integrated COHP (-ICOHP) of X-S interactions by comparing COHP below the Fermi level. The high-intensity negative below the Fermi level of the COHP analysis indicates X-S bonding well. Meanwhile, a small weakness in their bonding is suggested by a few antibonding interactions at the highest occupied bands, indicating an electronic instability. By combining the -ICOHP values of X-S interactions, we suggest that Si-S has stronger covalent bonding through orbital interactions with an -ICOHP value of -2.79 eV [Ge-S (-0.56 eV) and Sn-S bonds (-0.57 eV)]. The increased hybridization in LZXS means that the electron density of S atoms is gathered around X-S regions and thus away from the Li-ion diffusion channel. This effect reduces the electrostatic interaction of Li-ions with anion sublattice, leading to a lower Li-ion migration barrier.

The hybridization between transition metals and oxygen has been reported to play a critical role in lithium intercalation voltages and the activity of oxygen electrocatalysts.⁵³ The valuable hybridization information of the X cation and S anion can be further gleaned from sulfur 1s (S K-edge) XAS (Figure 7a), which can provide insight into the hybridization and measure the density of unoccupied states of S 2p states (S 2p holes) (Figure 7b). According to the calculated partial density

of states (PDOS) of S and Si in LZSiS (Figure 7b), the first and second peaks of the S K-edge originate from electronic transitions from the S 1s shell to the empty X cation ns (Si: n =3, Ge: n = 4, and Sn: n = 5) orbitals hybridized with S 2sp orbitals. The following broad features are assigned to S 2sp orbitals and S 2p states hybridized with the cation np orbitals. We found that the first and second features of the S K-edge undergo a pronounced edge downshift of -1.5 eV and a shape transformation going from Si to Ge/Sn. This observation is explained as a decrease in hybridization between X (nsp) and S (2p) states, which could increase the high electron density on S sites. This result is consistent with that of COHP in Figure 6d. Therefore, this point leads to strong electrostatic interaction between Li-ions and the host structure, increasing the Li-ion migration barrier. To further explain the lower migration barrier of Li diffusion in LZSiS, we calculated the Li K-edge XAS of LZXS and the PDOS of Li and S in LZSiS (Figure S3). According to the calculated PDOS of Li and S in LZSiS, the peaks of the Li K-edge correspond to the transition of the Li 1s electron to the hybridized state of the empty Li 2sp and S 2sp orbitals. Compared to LZSiS, the decreasing hybridization between Li and S orbitals in LZGS/LZSnS may suggest the strong electrostatic interaction between Li-ions and the host structure, which is consistent with the Li vacancy formation energy in Table 2. Therefore, Cl-NEB, COHP, and XAS calculations demonstrate that the lower Li-ion migration barrier in LZSiS owes much to a strong hybridization between Si and S atoms. Moreover, the variation in the Li-ion migration

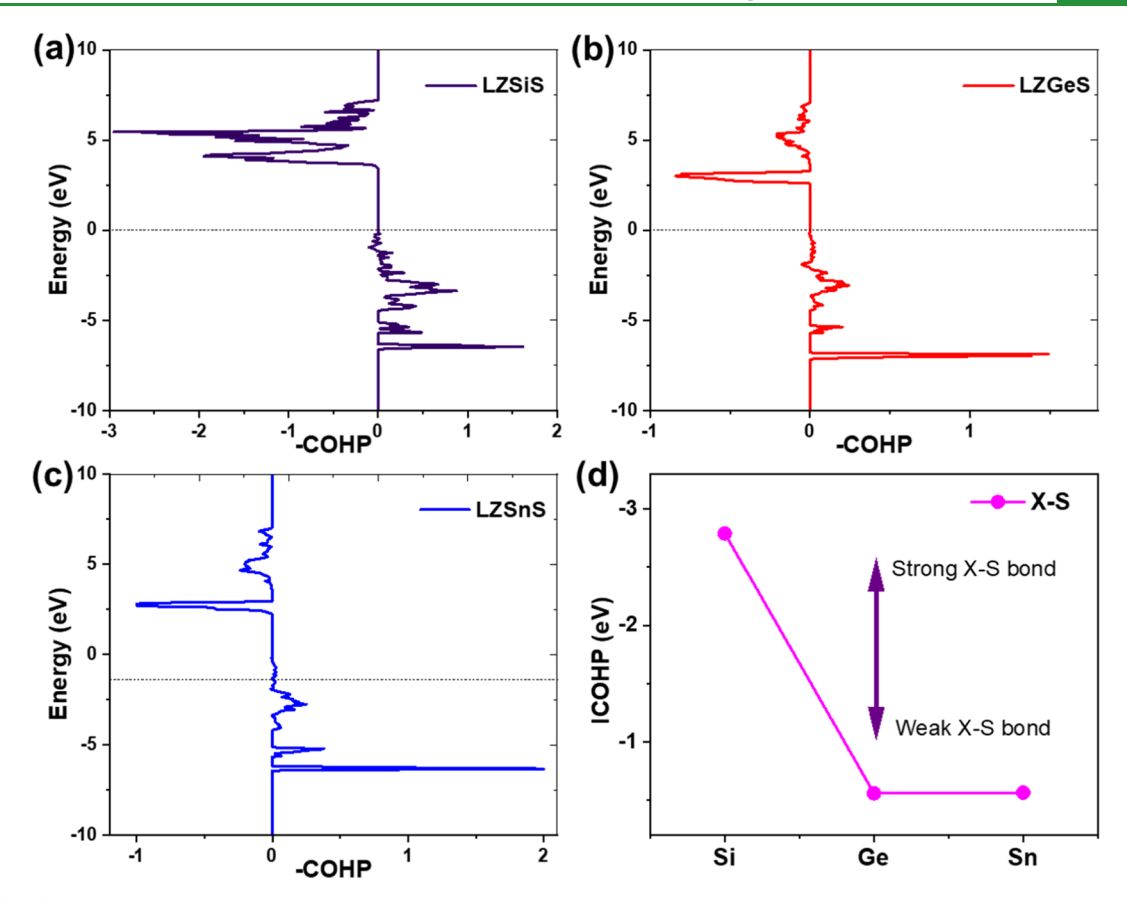


Figure 6. (a-c) Energy states of X-S hybridization bonding interaction against COHP in LZXS. The negative or positive values represent antibonding or bonding interactions. The horizontal dash lines represent the Fermi level. (d) –ICOHP (eV) of X-S hybridization bonding with different X^{4+} ions in LZXS.

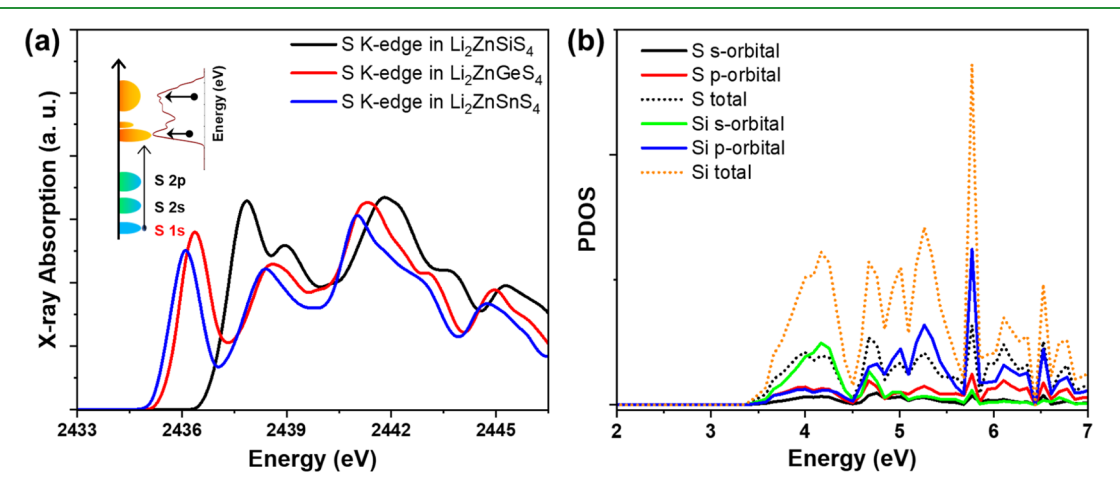


Figure 7. (a,b) Calculated S K-edge XAS of LZXS and PDOS of S and Si in LZSiS. The inset in Figure 6a is the schematic representation of an XAS spectrum for S atom.

barrier in the LZXS system highlights the importance of host cations in promoting high ionic conductivity.

4. CONCLUSIONS

In summary, we apply the DFT method together with the Materials Project data to evaluate new lithium thiosilicate conductors with a large range of aliovalent ion doping, a low Li-ion migration energy barrier in the diffusion channel, and a moderate electrochemical stability window. Interstitial Li-ions are the dominant defects on the anode side (0 V vs Li/Li⁺) and

Li vacancy becomes the dominant defect above 4.0 V. However, in LZXS, Li direct hopping via vacancy is equally important as interstitial migration by having almost the same migration barrier, but the high formation energy found for the Li vacancy suggests limited concentrations in the stoichiometric compound. The intrinsic concentrations of defects (the Li vacancy and interstitial) would need to be tuned by aliovalent doping. More importantly, we find that the structural tuning by isovalent X-site substitution within the LZXS framework has a large effect on the Li-ion migration barrier and phase stability but has a marginal effect on the

electrochemical stability. Among LZXS, LZSiS has a very low migration energy barrier (~0.24 eV). By comparing to LZSnS or LZGS, the significant shift of the S K-edge in LZSiS signifies stronger hybridization between Si and S orbitals. The increased hybridization of the Si and S orbitals implies high covalency of the Si—S bond, rendering a lower Li-ion migration barrier. This point suggests that structural tuning in sulfide materials by cation substitution within a given lattice structure to control hybridization between the cation and anion would enhance ionic conductivity. This work for the first time suggests that thiosilicates LZSiS with a low migration barrier and LZGS and LZSnS with acceptable migration barriers and good stability have a high potential for SSEs. We hope this work stimulates further experimental exploration within the crystal framework for fast Li-ion conductors.

ASSOCIATED CONTENT

5 Supporting Information

The Supporting Information is available free of charge at https://pubs.acs.org/doi/10.1021/acsami.1c24206.

Structural parameters for LZGS, TDOS of LZSiS with four different defects $(V_{Li}^-, Li_i^+, FP_{Li}^-, and FP_{Li}^+)$, electrochemical stability windows of LZXS, mixing chemical reactions of LZXS with cathodes, and mixing chemical reaction of LZXS with H_2O/CO_2 (PDF)

AUTHOR INFORMATION

Corresponding Authors

Bingkai Zhang — Guangzhou Key Laboratory of Clean Transportation Energy Chemistry, School of Chemical Engineering and Light Industry, Guangdong University of Technology, Guangzhou 510006, China; Email: zhangbk@gdut.edu.cn

Feng Pan — School of Advanced Materials, Peking University Shenzhen Graduate School, Shenzhen 518055, China; orcid.org/0000-0002-8216-1339; Email: panfeng@pku.edu.cn

Zhan Lin — Guangzhou Key Laboratory of Clean Transportation Energy Chemistry, School of Chemical Engineering and Light Industry, Guangdong University of Technology, Guangzhou 510006, China; Email: zhanlin@gdut.edu.cn

Author

Jiajie Zhong — Guangzhou Key Laboratory of Clean Transportation Energy Chemistry, School of Chemical Engineering and Light Industry, Guangdong University of Technology, Guangzhou 510006, China

Complete contact information is available at: https://pubs.acs.org/10.1021/acsami.1c24206

Notes

The authors declare no competing financial interest.

ACKNOWLEDGMENTS

This work was supported by the GuangDong Basic and Applied Basic Research Foundation (2020A1515110046).

■ REFERENCES

(1) Wang, C.; Liang, J.; Zhao, Y.; Zheng, M.; Li, X.; Sun, X. All-Solid-State Lithium Batteries Enabled by Sulfide Electrolytes: From

- Fundamental Research to Practical Engineering Design. *Energy Environ. Sci.* **2021**, *14*, 2577–2619.
- (2) Lin, Z.; Liu, T.; Ai, X.; Liang, C. Aligning Academia and Industry for Unified Battery Performance Metrics. *Nat. Commun.* **2018**, *9*, 5262–5266.
- (3) Xiao, Y.; Turcheniuk, K.; Narla, A.; Song, A.-Y.; Ren, X.; Magasinski, A.; Jain, A.; Huang, S.; Lee, H.; Yushin, G. Electrolyte Melt Infiltration for Scalable Manufacturing of Inorganic All-Solid-State Lithium-Ion Batteries. *Nat. Mater.* **2021**, *20*, 984–990.
- (4) Schwietert, T. K.; Arszelewska, V. A.; Wang, C.; Yu, C.; Vasileiadis, A.; de Klerk, N. J. J.; Hageman, J.; Hupfer, T.; Kerkamm, I.; Xu, Y.; van der Maas, E.; Kelder, E. M.; Ganapathy, S.; Wagemaker, M. Clarifying the Relationship between Redox Activity and Electrochemical Stability in Solid Electrolytes. *Nat. Mater.* **2020**, *19*, 428–435.
- (5) Zhang, B.; Tan, R.; Yang, L.; Zheng, J.; Zhang, K.; Mo, S.; Lin, Z.; Pan, F. Mechanisms and Properties of Ion-Transport in Inorganic Solid Electrolytes. *Energy Storage Mater.* **2018**, *10*, 139–159.
- (6) Amores, M.; El-Shinawi, H.; McClelland, I.; Yeandel, S. R.; Baker, P. J.; Smith, R. I.; Playford, H. Y.; Goddard, P.; Corr, S. A.; Cussen, E. J. $\rm Li_{1.5}La_{1.5}MO_6$ (M=W6+ $^{\rm T}$ e6+ $^{\rm la}$ s aNew Series of Lithium -RichDouble Perovskites for All -Solid-StateLithium -IonBatteries. *Nat. Commun.* **2020**, *11*, 6392.
- (7) Zhang, B.; Zhong, J.; Zhang, Y.; Yang, L.; Yang, J.; Li, S.; Wang, L.-W.; Pan, F.; Lin, Z. Discovering a New Class of Fluoride Solid-Electrolyte Materials Via Screening the Structural Property of Li-Ion Sublattice. *Nano Energy* **2021**, *79*, 105407.
- (8) Lu, Y.; Alonso, J. A.; Yi, Q.; Lu, L.; Wang, Z. L.; Sun, C. A High-Performance Monolithic Solid-State Sodium Battery with Ca²⁺ Doped Na₃Zr₂Si₂PO₁₂ Electrolyte. *Adv. Energy Mater.* **2019**, *9*, 1901205.
- (9) Wang, J.; Sun, C.-W.; Gong, Y.-D.; Zhang, H.-R.; Alonso, J. A.; Fernández-Díaz, M. T.; Wang, Z.-L.; Goodenough, J. B. Imaging the diffusion pathway of Al^{3+} ion in NASICON-type $(Al_{0.2}Zr_{0.8})_{20/19}Nb-(PO_4)_3$ as electrolyte for rechargeable solid-state Al batteries. *Chin. Phys. B* **2018**, *27*, 128201.
- (10) Ong, S. P.; Mo, Y.; Richards, W. D.; Miara, L.; Lee, H. S.; Ceder, G. Phase Stability, Electrochemical Stability and Ionic Conductivity of the $\text{Li}_{10\pm 1}\text{MP}_2\text{X}_{12}$ (M = Ge, Si, Sn, Al or P, and X = O, S or Se) Family of Superionic Conductors. *Energy Environ. Sci.* **2013**, *6*, 148–156.
- (11) Mo, Y.; Ong, S. P.; Ceder, G. First Principles Study of the $\rm Li_{10}GeP_2S_{12}$ Lithium Super Ionic Conductor Material. *Chem. Mater.* **2012**, 24, 15–17.
- (12) Mo, Y.; Ong, S. P.; Ceder, G. First Principles Study of the $Li_{10}GeP_2S_{12}$ Lithium Super Ionic Conductor Material. *Chem. Mater.* **2012**, 24, 15–17.
- (13) Bernges, T.; Culver, S. P.; Minafra, N.; Koerver, R.; Zeier, W. G. Competing Structural Influences in the Li Superionic Conducting Argyrodites Li_6PS_5 -xSexBr $(0 \le x \le 1)$ Upon Se Substitution. *Inorg. Chem.* **2018**, *57*, 13920–13928.
- (14) Deiseroth, H.-J.; Kong, S.-T.; Eckert, H.; Vannahme, J.; Reiner, C.; Zaiß, T.; Schlosser, M. Li₆PS₅X: A Class of Crystalline Li-Rich Solids with an Unusually High Li⁺ Mobility. *Angew. Chem., Int. Ed.* **2008**, *47*, 755–758.
- (15) Maldonado-Manso, P.; Losilla, E. R.; Martínez-Lara, M.; Aranda, M. A. G.; Bruque, S.; Mouahid, F. E.; Zahir, M. High Lithium Ionic Conductivity in the Li_{1+x}Al_xGe_yTi_{2-x-y}(PO₄)₃ NASICON Series. *Chem. Mater.* **2003**, *15*, 1879–1885.
- (16) Abramchuk, M.; Voskanyan, A. A.; Arinicheva, Y.; Lilova, K.; Subramani, T.; Ma, Q.; Dashjav, E.; Finsterbusch, M.; Navrotsky, A. Energetic Stability and Its Role in the Mechanism of Ionic Transport in NASICON-Type Solid-State Electrolyte Li_{1+x}Al_xTi_{2-x}(PO₄)₃. *J. Phys. Chem. Lett.* **2021**, *12*, 4400–4406.
- (17) Zhang, B.; Lin, Z.; Dong, H.; Wang, L.-W.; Pan, F. Revealing Cooperative Li-ion Migration in $\text{Li}_{1+x}\text{Al}_x\text{Ti}_{2-x}(\text{PO}_4)_3$ Solid State Electrolytes with High Al Doping. *J. Mater. Chem. A* **2020**, *8*, 342–348.
- (18) Wu, J.-F.; Chen, E.-Y.; Yu, Y.; Liu, L.; Wu, Y.; Pang, W. K.; Peterson, V. K.; Guo, X. Gallium-Doped Li₇La₃Zr₂O₁₂ Garnet-Type

- Electrolytes with High Lithium-Ion Conductivity. ACS Appl. Mater. Interfaces 2017, 9, 1542–1552.
- (19) Buannic, L.; Orayech, B.; López Del Amo, J.-M.; Carrasco, J.; Katcho, N. A.; Aguesse, F.; Manalastas, W.; Zhang, W.; Kilner, J.; Llordés, A. Dual Substitution Strategy to Enhance Li⁺ Ionic Conductivity in Li₇La₃Zr₂O₁₂ Solid Electrolyte. *Chem. Mater.* **2017**, 29, 1769–1778.
- (20) Sun, C.; Liu, J.; Gong, Y.; Wilkinson, D. P.; Zhang, J. Recent Advances in All-Solid-State Rechargeable Lithium Batteries. *Nano Energy* **2017**, *33*, *363*–386.
- (21) Zheng, C.; Li, L.; Wang, K.; Wang, C.; Zhang, J.; Xia, Y.; Huang, H.; Liang, C.; Gan, Y.; He, X.; Tao, X.; Zhang, W. Interfacial Reactions in Inorganic All-Solid-State Lithium Batteries. *Batteries Supercaps* **2020**, *4*, 8–38.
- (22) Zheng, C.; Zhang, J.; Xia, Y.; Huang, H.; Gan, Y.; Liang, C.; He, X.; Tao, X.; Zhang, W. Unprecedented Self-Healing Effect of Li₆PS₅Cl-Based All-Solid-State Lithium Battery. *Small* **2021**, *17*, 2101326.
- (23) Zhang, J.; Li, L.; Zheng, C.; Xia, Y.; Gan, Y.; Huang, H.; Liang, C.; He, X.; Tao, X.; Zhang, W. Silicon-Doped Argyrodite Solid Electrolyte Li₆PS₅I with Improved Ionic Conductivity and Interfacial Compatibility for High-Performance All-Solid-State Lithium Batteries. ACS Appl. Mater. Interfaces 2020, 12, 41538–41545.
- (24) Tian, Y.; Shi, T.; Richards, W. D.; Li, J.; Kim, J. C.; Bo, S.-H.; Ceder, G. Compatibility Issues between Electrodes and Electrolytes in Solid-State Batteries. *Energy Environ. Sci.* **2017**, *10*, 1150–1166.
- (25) Li, G.; Chu, Y.; Zhou, Z. From AgGaS₂ to Li₂ZnSiS₄: Realizing Impressive High Laser Damage Threshold Together with Large Second-Harmonic Generation Response. *Chem. Mater.* **2018**, *30*, 602–606
- (26) Zhang, J.-H.; Clark, D. J.; Brant, J. A.; Rosmus, K. A.; Grima, P.; Lekse, J. W.; Jang, J. I.; Aitken, J. A. α -Li₂ZnGeS₄: A Wide-Bandgap Diamond-Like Semiconductor with Excellent Balance between Laser-Induced Damage Threshold and Second Harmonic Generation Response. *Chem. Mater.* **2020**, *32*, 8947–8955.
- (27) Lekse, J. W.; Leverett, B. M.; Lake, C. H.; Aitken, J. A. Synthesis, Physicochemical Characterization and Crystallographic Twinning of Li₂ZnSnS₄. *J. Solid State Chem.* **2008**, *181*, 3217–3222.
- (28) Kresse, G.; Furthmüller, J. Efficient Iterative Schemes for Ab Initio Total-Energy Calculations Using a Plane-Wave Basis Set. *Phys. Rev. B: Condens. Matter Mater. Phys.* **1996**, *54*, 11169–11186.
- (29) Perdew, J. P.; Chevary, J. A.; Vosko, S. H.; Jackson, K. A.; Pederson, M. R.; Singh, D. J.; Fiolhais, C. Atoms, Molecules, Solids, and Surfaces: Applications of the Generalized Gradient Approximation for Exchange and Correlation. *Phys. Rev. B* **1992**, *46*, 6671–6687.
- (30) Kresse, G.; Furthmüller, J. Efficiency of Ab-Initio Total Energy Calculations for Metals and Semiconductors Using a Plane-Wave Basis Set. *Comput. Mater. Sci.* **1996**, *6*, 15–50.
- (31) Blöchl, P. E. Projector Augmented-Wave Method. *Phys. Rev. B* **1994**, *50*, 17953–17979.
- (32) Henkelman, G.; Uberuaga, B. P.; Jónsson, H. A Climbing Image Nudged Elastic Band Method for Finding Saddle Points and Minimum Energy Paths. *J. Phys. Chem. A* **2000**, *113*, 9901–9904.
- (33) Kirklin, S.; Meredig, B.; Wolverton, C. High-Throughput Computational Screening of New Li-Ion Battery Anode Materials. *Adv. Energy Mater.* **2013**, *3*, 252–262.
- (34) Wolverton, C.; Siegel, D. J.; Akbarzadeh, A. R.; Ozoliņš, V. Discovery of Novel Hydrogen Storage Materials: An Atomic Scale Computational Approach. *J. Phys.: Condens. Matter* **2008**, *20*, 064228.
- (35) Richards, W. D.; Miara, L. J.; Wang, Y.; Kim, J. C.; Ceder, G. Interface Stability in Solid-State Batteries. *Chem. Mater.* **2016**, 28, 266–273.
- (36) Ong, S. P.; Wang, L.; Kang, B.; Ceder, G. Li-Fe-P-O₂ Phase Diagram from First Principles Calculations. *Chem. Mater.* **2008**, 20, 1798–1807.
- (37) Ong, S. P.; Mo, Y.; Richards, W. D.; Miara, L.; Lee, H. S.; Ceder, G. Phase Stability, Electrochemical Stability and Ionic Conductivity of the $Li_{10+/-1}MP_2X_{12}$ (M = Ge, Si, Sn, Al or P, and X

- = O, S or Se) Family of Superionic Conductors. *Energy Environ. Sci.* **2013**, *6*, 148–156.
- (38) Ong, S. P.; Richards, W. D.; Jain, A.; Hautier, G.; Kocher, M.; Cholia, S.; Gunter, D.; Chevrier, V. L.; Persson, K. A.; Ceder, G. Python Materials Genomics (Pymatgen): A Robust, Open-Source Python Library for Materials Analysis. *Comput. Mater. Sci.* **2013**, *68*, 314–319.
- (39) Banerjee, S.; Zhang, X.; Wang, L.-W. Motif-Based Design of an Oxysulfide Class of Lithium Superionic Conductors: Toward Improved Stability and Record-High Li-Ion Conductivity. *Chem. Mater.* **2019**, *31*, 7265–7276.
- (40) Wong, L. L.; Phuah, K. C.; Dai, R.; Chen, H.; Chew, W. S.; Adams, S. Bond Valence Pathway Analyzer-An Automatic Rapid Screening Tool for Fast Ion Conductors within softBV. *Chem. Mater.* **2021**, 33, 625–641.
- (41) He, Z.; Zhang, B.; Zhong, J.; Lin, Z.; Pan, F. Tuning Site Energy by XO₆ Units in LiX₂(PO₄)₃ Enables High Li Ion Conductivity and Improved Stability. *ACS Appl. Mater. Interfaces* **2021**, 13, 50948–50956.
- (42) Xiao, Y.; Wang, Y.; Bo, S.-H.; Kim, J. C.; Miara, L. J.; Ceder, G. Understanding Interface Stability in Solid-State Batteries. *Nat. Rev. Mater.* **2020**, *5*, 105–126.
- (43) Han, F.; Zhu, Y.; He, X.; Mo, Y.; Wang, C. Electrochemical Stability of Li₁₀GeP₂S₁₂ and Li₇La₃Zr₂O₁₂ Solid Electrolytes. *Adv. Energy Mater.* **2016**, *6*, 1501590.
- (44) Zhu, Y.; He, X.; Mo, Y. First Principles Study of Electrochemical and Chemical Stability of the Solid Electrolyte-Electrode Interfaces in All-Solid-State Li-Ion Batteries. *J. Mater. Chem. A* **2016**, 4, 3253–3266.
- (45) Zhang, B.; Zhong, J.; Pan, F.; Lin, Z. Potential Solid-State Electrolytes with Good Balance between Ionic Conductivity and Electrochemical Stability: $\text{Li}_{5-x}M_{1-x}M_x'O_4$ (M = Al and Ga and M' = Si and Ge). ACS Appl. Mater. Interfaces **2021**, 13, 61296–61304.
- (46) Kamaya, N.; Homma, K.; Yamakawa, Y.; Hirayama, M.; Kanno, R.; Yonemura, M.; Kamiyama, T.; Kato, Y.; Hama, S.; Kawamoto, K.; Mitsui, A. A Lithium Superionic Conductor. *Nat. Mater.* **2011**, *10*, 682–686.
- (47) Wang, S.; Bai, Q.; Nolan, A. M.; Liu, Y.; Gong, S.; Sun, Q.; Mo, Y. Lithium Chlorides and Bromides as Promising Solid-State Chemistries for Fast Ion Conductors with Good Electrochemical Stability. *Angew. Chem., Int. Ed.* **2019**, *58*, 8039–8043.
- (48) Li, X.; Liang, J.; Luo, J.; Norouzi Banis, M.; Wang, C.; Li, W.; Deng, S.; Yu, C.; Zhao, F.; Hu, Y.; Sham, T.-K.; Zhang, L.; Zhao, S.; Lu, S.; Huang, H.; Li, R.; Adair, K. R.; Sun, X. Air-Stable Li3incl6 Electrolyte with High Voltage Compatibility for All-Solid-State Batteries. *Energy Environ. Sci.* **2019**, *12*, 2665–2671.
- (49) Li, Y.; Zhou, W.; Xin, S.; Li, S.; Zhu, J.; Lü, X.; Cui, Z.; Jia, Q.; Zhou, J.; Zhao, Y.; Goodenough, J. B. Fluorine-Doped Antiperovskite Electrolyte for All-Solid-State Lithium-Ion Batteries. *Angew. Chem.* **2016**, *128*, 10119–10122.
- (50) Ahn, B. T.; Huggins, R. A. Synthesis and Lithium Conductivities of Li₂SiS₃ and Li₄SiS₄. *Mater. Res. Bull.* **1989**, 24, 889–897.
- (51) He, X.; Zhu, Y.; Mo, Y. Origin of Fast Ion Diffusion in Super-Ionic Conductors. *Nat. Commun.* **2017**, *8*, 15893.
- (52) Lang, B.; Ziebarth, B.; Elsässer, C. Lithium Ion Conduction in $LiTi_2(PO_4)_3$ and Related Compounds Based on the Nasicon Structure: A First-Principles Study. *Chem. Mater.* **2015**, 27, 5040–5048.
- (53) Frati, F.; Hunault, M. O. J. Y.; de Groot, F. M. F. Oxygen K-Edge X-Ray Absorption Spectra. Chem. Rev. 2020, 120, 4056-4110.
- (54) Dronskowski, R.; Bloechl, P. E. Crystal Orbital Hamilton Populations (COHP): Energy-Resolved Visualization of Chemical Bonding in Solids Based on Density-Functional Calculations. *J. Phys. Chem.* **1993**, 97, 8617–8624.
- (55) Deringer, V. L.; Tchougréeff, A. L.; Dronskowski, R. Crystal Orbital Hamilton Population (COHP) Analysis as Projected from Plane-Wave Basis Sets. *J. Phys. Chem. A* **2011**, *115*, 5461–5466.